JOURNAL OF MATERIALS SCIENCE **40** (2005) 5427 – 5433

Prediction of fatigue limit of induction surface hardened 1.05Cr–0.23Mo steel alloy using extreme value statistics

BYOUNG-HO CHOI
Department of Civil and Materials Engineering, University of Illinois at Chicago, Chicago, IL 60607, USA

SAM-HONG SONG
Department of Mechanical Engineering, Korea University, Seoul, Republic of Korea

Fatigue characteristics of the surface hardened steel are different from that of normal steel, so the prediction of the fatigue limit of surface hardened steel is very complicated. In this paper, specimens are tested using rotary bending, and the surface of 1.05Cr–0.23Mo steel alloy is hardened by induction surface hardening. Variation of the distribution of microvickers hardness and residual stress is discussed, and the difference of S-N diagram between surface hardened steel and unhardened steel is examined. The maximum defect size of surface hardened specimen is calculated by the extreme value statistics to predict conservative fatigue limit. Actual shape of defect in the specimen is three dimensional, so a conversion method from 2D to 3D defect size based on examination volume and inclusion size is used to predict statistical maximum defect size. The predicted results can be defined as a lower fatigue limit which may be useful to predict conservative fatigue limit of surface hardened specimen.

1. Introduction

Unpredictable failure due to inclusions or defects which are generated during heat treatment of surface hardening may occur in many cases. Therefore, there have been many studies [1–5] about the effect of inclusions or defects on the fatigue limit of surface hardened steel. However, most existing studies are based on an evaluation using a 2-D crack shape and stress concentration factors. Hence, the quantitative evaluation of inclusions is necessary to establish a quantitative prediction of fatigue limit. For a better prediction of fatigue limit, it is important to classify major factors and use an appropriate parameter for 3-D defects or inclusions. Murakami [6, 7] suggested $\sqrt{\text{area}}$ as a fracture mechanics parameter and evaluated the fatigue limit of high strength steel using the parameter.

Mechanical factors such as the position and size of inclusions, a hardness distribution, the evaluation of residual stress and the selection of dangerous area can be considered as the influential factors for the fatigue limit of surface hardened steel. Song *et al.* [8] reported the actual distribution of inclusions observed by fractography. For the precise prediction of the fatigue limit, statistics with extreme number can be applied to obtain the maximum inclusion size [9].

In this paper, the 3-D maximum inclusion size for induction surface hardened steel is calculated using extreme value statistics with extreme values and the risk area for induction surface hardened steel is suggested. In addition, the fatigue limit prediction according to the obtained results is evaluated and compared with the experimental results.

2. Experiments

The material used in this study is a commercial 1.05Cr–0.23Mo steel alloy which is widely used for manufacturing gears and shafts. Chemical composition obtained by X-ray spectra analysis is shown in Table I. To eliminate the effect of initial residual stress and metallurgical structure, specimens were machined after annealing (1 h at 850°C and furnace cooling). In Table II, mechanical properties obtained on the test material are shown.

Machined test specimens are shown in Fig. 1. The surface of the specimen is polished using sand paper and Alumina oxide from #200 to #2000. The process conditions for induction surface hardening are 50 kW of power, 1.6 A of current and variable time with a single shot coil. Specimens are named BM for base metal, and H1, H6 and HF for surface hardened steel (effective case depths are 1.1, and 1.6 mm and full diameter respectively). The additional classification, SS, stands for smooth specimen

The test machine is an Ono-type 4-point rotary bending fatigue test machine which can produce 98N-m of maximum bending moment. The rotation speed is

0022–2461
DOI: 10.1007/s10853-005-2800-3

TABLE I The chemical composition of used material

Cr-Mo Steel Alloy, SCM440 (wt%)				
C	Si	Mn	Cr	Mo
0.41	0.25	0.68	1.05	0.23

TABLE II The mechanical property of used material

Yield Stress, σ_y (MPa)	Ultimate Stress, σ_u (MPa)	Micro Vickers Hardness, *HV*
556.8	664.3	215

3000 rpm and the applied stress ratio (R) is −1(fully reversed).

3. Results and discussion

3.1. Distribution of microvickers hardness and residual stress

The distribution of hardness inside the material is very important for determining the depth of surface hardening. To determine the level of surface hardening, an etching method is used for qualitative analysis and microvickers hardness measurements are used for quantitative analysis. In this paper, the microvickers hardness method is used for measuring the effective hardness depth. The microvickers hardness of annealed base metal was measured at about HV 215. The hardness at the surface to all hardened specimens is HV 560 with the maximum hardness of approximately HV 570 at 0.1 mm depth from surface for H6 and H1 specimen. The reason why the position of maximum hardness is located under surface is incomplete quenching during cooling from high temperature. The occurrence of non-martensite due to heat treatment is the main reason of the formation of hardness gradient. On the other hand, in the case of FH specimens, the hardness measured from surface to core is almost the same, HV 560–575. The hardness ratio (*HR*) is defined from the ratio of the effective case depth (*ECD*) and the radius of specimen (*R*) [10].

$$HR = \frac{ECD}{R} \tag{1}$$

The effective case depth for H6 is 1.6 mm and full hardened depth is 2.4 mm. So, in this case, the hardness ratio is 0.35. Moreover, the hardness ratios for H1 and HF specimen are calculated as 0.24 and 1 respectively.

TABLE III Residual stress and microvickers hardness obtained by experiment

	Specimen		
Index	HF	H1	H6
Surface hardness (HV)	560	560	560
Maximum hardness (HV)	575	570	570
Effective case depth (mm)	N/A	1.1	1.6
Full case depth (mm)	4.5	2.0	2.4
Hardening Ratio	1	0.24	0.35
Residual stress at surface (MPa)	−322.8	−451.1	−383.4
Maximum residual stress (MPa)	−416.9	−596.6	−434.6

The distribution of the axial residual stress of induction surface hardened smooth specimen can be measured by X-ray diffraction analysis. After measuring residual stress at an exposed surface, electro-polishing is applied for the elimination of a small amount (0.1–0.2 mm) of hardened layer. By repetition of the measurement, the residual stress distribution can be obtained. For the X-ray diffraction analysis, the characteristic X-ray target is Cr–Kα , the irradiated area is 4×2 mm^2 and scanning speed is 8°/min.

Compressive residual stress decreases from surface to core, and it shows the same tendency as the microvickers hardness distribution. The measured compressive residual stresses at surface of specimen are 383.4, 451.1 MPa for H6 and H1 specimens, respectively. The residual stress increases up to 0.3 mm from surface and decreases slowly to core. For the HF specimen, the compressive residual stress at surface is 322 MPa, which is lower compared with the compressive residual stress at surface for surface hardened specimens. In addition, the decreasing rate of measured residual stress for HF specimen is faster than that for the surface hardened specimen. In Fig. 2, the distribution of residual stress is shown. In Table III, measured results of residual stress and microvickers hardness for each specimen are shown.

3.2. Variation of fatigue behavior due to inclusions

The determination of fatigue limit is carried out by measuring the applied stress level for non-fractured specimens after 10^7 cycles. Fatigue limit is calculated mainly

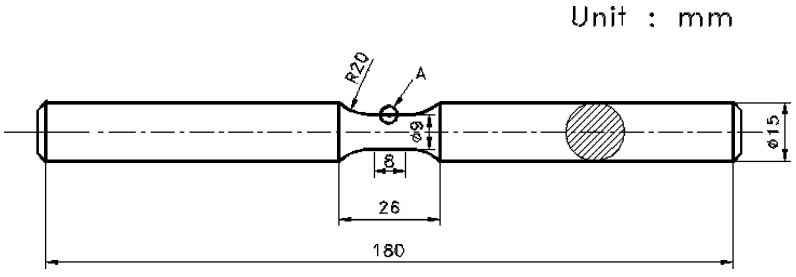

Figure 1 Geometry of rotary bending fatigue specimen.

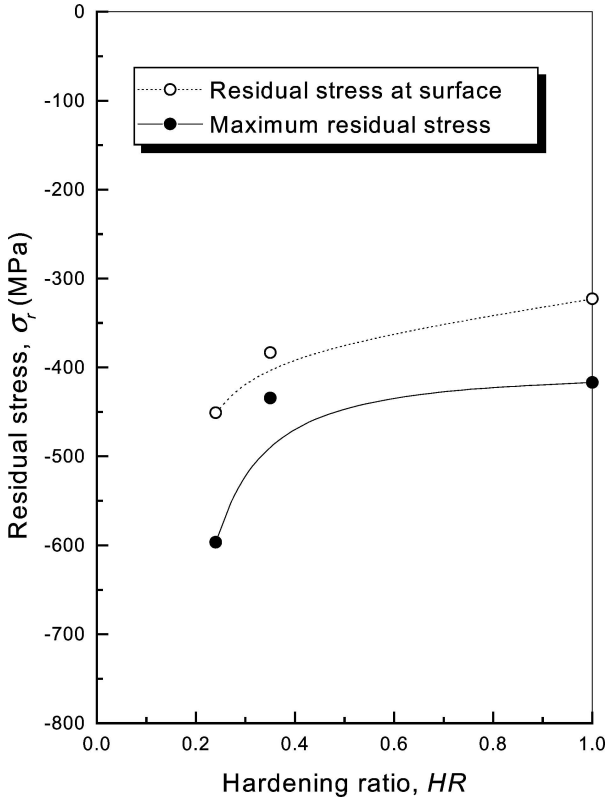

Figure 2 Relationship between residual stress and hardening ratio.

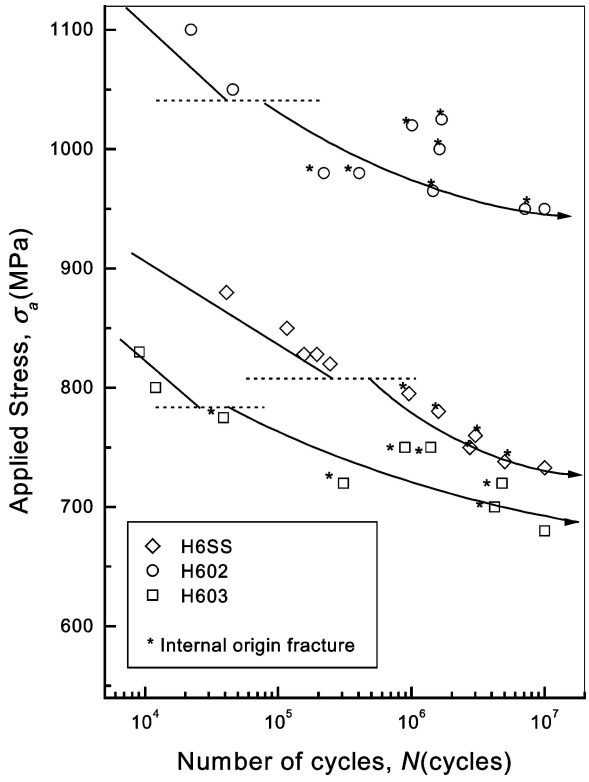

Figure 3 Measured *S-N* behaviour.

based on the standard JSME S002 with the stair-case method. Based on the standard's recommendation, fatigue limit can be calculated with 6 specimens for 50% probability of failure. However, in this experiment, the application of the suggested method is impossible because of the failure from inclusions at high cyclic lives. Hence, the fatigue limit is, in this paper, defined as the stress level at which a specimen is not fractured at 10^7 cycles.

The S-N diagrams obtained from the experiments on the surface hardened steel are shown in Fig. 3. Observations of fracture surface show that crack initiation sites are located at surface for short lives and at internal fish-eyes for long lives. High strength steels for where the S-N diagram can be divided into two steps show very similar fatigue characteristics. The S-N curves for the smooth specimen subjected to induction hardening show two steps, and the reason is that silver-colored fish-eyes (internal crack origins) are observed as the initiation position of fatigue cracks in the long life regime [7, 11, 12]. Song *et al*. also reported the distribution of fracture origins for surface hardened steel [8].

3.3. Estimation of maximum inclusion size using extreme values statistics

The estimation of the maximum inclusion size using extreme values statistics was suggested by Murakami *et al*. [9]. This method can be used for the practical purpose with sufficient accuracy. Usuki and Murakami [13] suggested the risk area as 10% of the diameter from the surface for high strength steel. However, from experiments, the distribution of fracture origins for surface hardened steel is wider than that for high strength steel [8]. So, according to experimental observation, the risk area for surface hardened steel is suggested as 20% of diameter in this paper. Hence, according to the hardening depth, the position and the size of examination area is changed. In Fig. 4, the definitions of risk area and actual values for the induction surface hardened specimen are shown.

The test specimen was cut perpendicular to the direction of principal stress and the cut cross section was polished for accurate examination of inclusion. According to the magnification and size of observed area, the examination area is defined. After determining the examination area of specific position, the maximum size of inclusion for that area can be obtained. The same measurement for different positions with the defined examination area is executed. After checking sufficient positions for each specimen, distributions of the maximum sizes of inclusion were plotted based on extreme values statistics. In Figs 5, 6 and 7, statistical distributions for each specimen are shown. Equations of the statistics with extreme values for each specimen are as follows.

$$\sqrt{area}_{\max} = 3.77 \cdot y + 7.585 \,(\text{HF specimen}) \quad (2)$$

$$\sqrt{area}_{\max} = 2.18 \cdot y + 5.302 \,(\text{H1 specimen}) \quad (3)$$

$$\sqrt{area}_{\max} = 1.58 \cdot y + 6.973 \,(\text{H6 specimen}) \quad (4)$$

Here, $\sqrt{area}_{\max}$ is the maximum size of inclusion and y is the normalized variable. The normalized variable can be expressed as follows.

$$y = -\ln\left(-\ln\frac{T-1}{T}\right) \quad (5)$$

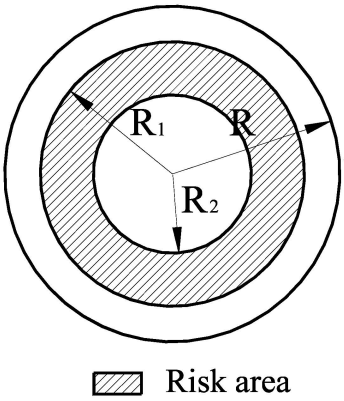

Specimen \ Index	Observed internal crack origin position (*mm*)	R_1 (*mm*)	R_2 (*mm*)	S^* (*mm*)
HF	0.44 ~ 1.02	4.5	3.6	22.90
H1	1.52 ~ 1.63	3.4	2.5	16.68
H6	1.59 ~ 1.99	3.0	2.1	14.42

* $S = \pi \cdot \left(R_1^2 - R_2^2\right)$

Figure 4 Selection of examination area for each specimen.

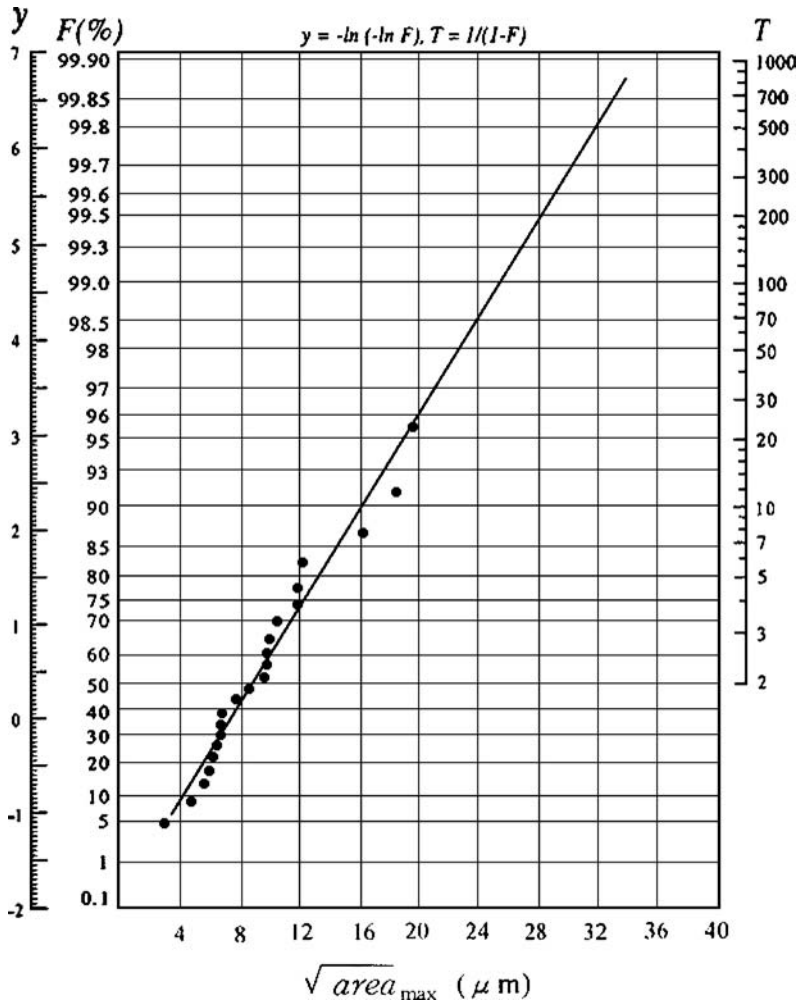

Figure 5 Statistical distribution of $\sqrt{area}_{\max}$ for HF specimen.

where, $T = \frac{S+S_0}{S_0}$ is the return period, S is target area which is the same as risk area of the specimen and S_0 is individual examination area of actual observation.

In Table IV, each parameter calculated from the above equations, and predicted maximum sizes for the calculated return period are shown. As a result, the distribution of $\sqrt{area}_{\max}$ for HF specimen is different from

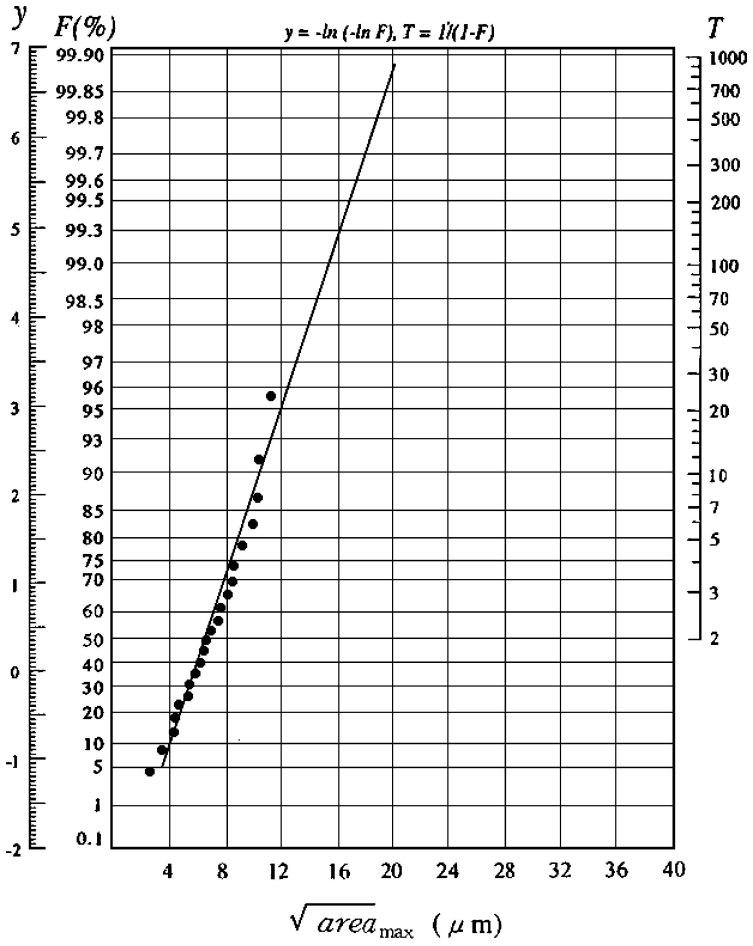

Figure 6 Statistical distribution of $\sqrt{area}_{max}$ for H1 specimen.

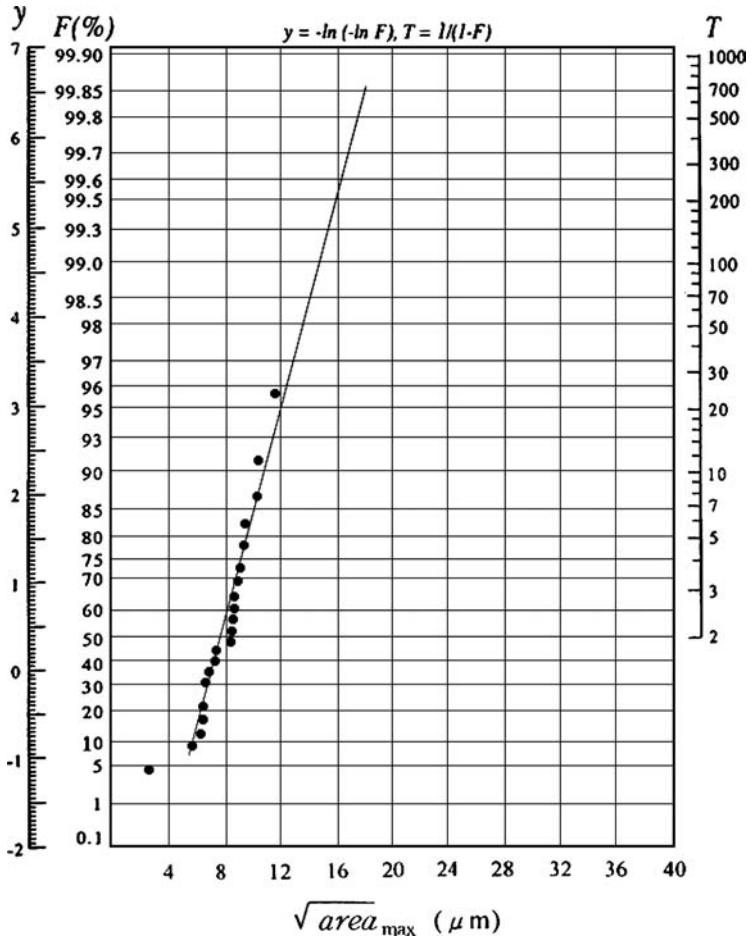

Figure 7 Statistical distribution of $\sqrt{area}_{max}$ for H6 specimen.

TABLE IV Calculated result of $\sqrt{area}_{\max}$ for each specimen

Index	Specimen		
	HF	H1	H6
Examination area, S_0 (mm^2)	0.06229	0.06229	0.06229
Rick section from surfac (mm)	0–0.9	1.1–2.0	1.5–2.4
Target area, S (mm^2)	22.90	16.68	14.42
Return period for 2D, T	368.6	268.8	232.5
$\sqrt{area}_{\max}$ by 2D method (μm)	29.85	17.49	15.58

that for H6 and H1 specimen. The predicted value of $\sqrt{area}_{\max}$ for HF is larger than the value for H1 and H6 specimen.

3.4. Evaluation of fatigue limit using 3-D maximum inclusion size

The values calculated above are based on a 2-D analysis. Toriyama *et al*. [12] suggested the method of evaluating 3-D maximum inclusion size using extreme values statistics. According to the proposed method, the definition of return period is changed as follows.

$$T = \frac{V + V_0}{V_0} \tag{6}$$

where, V is target volume and V_0 is examined volume. Target volume for rotary bending specimens can be calculated as $V = S \cdot l$ and examined volume can be expressed as $V_0 = S_0 \cdot h$. Here, l is the length of the parallel part of the specimen and h is virtual thickness which can be expressed as follows.

$$h = \sum_{j=1}^{n} \frac{\sqrt{area}_{\max,j}}{n} \tag{7}$$

where, n is the number of examination areas. In addition, the return period for multiple samples (N) can be expressed as follows.

$$T(N) = \frac{N \cdot V + V_0}{V_0} \cong \frac{N \cdot V}{V_0} \tag{8}$$

In Table V, the results of 3-D maximum inclusion size for the number of samples are shown. The fatigue limit prediction with the proposed equation for induction surface hardened specimen by Song and Choi [8] is done using the calculated 3-D maximum inclusion sizes. In this calculation, residual stress and microvickers hardness of R_2 position (see Fig. 4) are used for conservative prediction of fatigue limit. In Fig. 8, predicted results are shown compared with experimental results.

The predicted value can be regarded as a lower level of the fatigue limit. Statistically, for a larger number of sample specimens, the predicted results will become smaller and conservative. In this experiment, the lifetime for the fatigue limit is defined as 10^7 cycles, but

TABLE V Prediction of fatigue limit using $\sqrt{area}_{\max}$ by specimen number

Index	Specimen		
	HF	H1	H6
Virtual thickness, h (mm)	9.444	6.853	7.807
Examination volume, V_0 (mm^2)	0.5883	0.4268	0.4863
Target volume, V (mm^2)	183.2	133.44	115.36
$\sqrt{area}_{\max}$ by 3D method (μm)	29.23	17.83	15.62
$N = 1$			
Return period, $T(4)$	312.4	313.6	238.2
$\sqrt{area}_{\max}(1)(\mu$m)	29.23	17.83	15.62
Predicted Fatigue limit, $\sigma_w(1)$ (MPa)	793.3	367.4	374.1
$N = 10$			
Return period, $T(10)$	3124	3136	2382
$\sqrt{area}_{\max(10)}(\mu$m)	37.92	22.85	19.26
Predicted Fatigue limit, $\sigma_w(10)$ (MPa)	766.5	350.7	360.7
$N = 100$			
Return period, $T(100)$	31240	31360	23820
$\sqrt{area}_{\max}(\mu$m)	46.60	27.87	22.90
Predicted Fatigue limit $\sigma_w(100)$ (MPa)	746.2	340.6	349.7

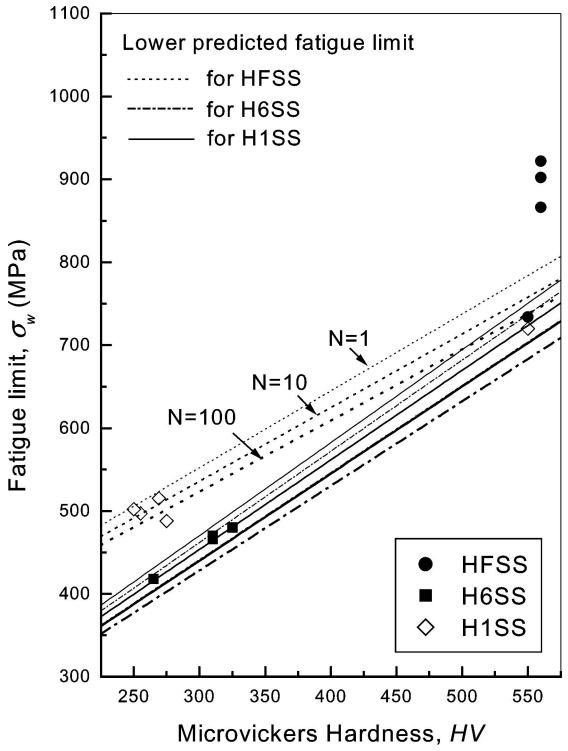

Figure 8 The relation between fatigue strength and microvickers hardness by the prediction of $\sqrt{area}_{\max}$.

many failures of high strength steel at very high lifetime have been reported [14, 15]. Hence, the actual fatigue limit of high strength steel and surface hardened steel may be lower than experimental results for 10^7 cycles. In that sense, the difference between experimental result and the prediction of fatigue limit based on the 3-D maximum inclusion size can be explained, and this method can be used as an effective method

for conservative prediction of fatigue limit. In addition, in this paper, predicted results for HF specimen are more conservative than the results for H6 and H1 specimen. It is explained that high strength steel (HF specimen) can be failed at much longer lifetime compared with surface hardened specimen (H6 and H1 specimen)

4. Conclusion

In this paper, the fatigue characteristics of surface hardened a Cr-Mo steel alloy are observed, and the statistical distribution of micro defects in the surface hardened specimen is examined. Using these experimental results and a fracture mechanics parameter, the prediction of lower fatigue limits for the surface hardened smooth specimen is executed.

(1) Using extreme values statistics, the possible maximum size of defect which can be found in the surface hardened specimen is calculated. Considering the position of fatigue crack initiation, the concept of risk areas is introduced $D = 2.1 - 3.0$ mm, $D = 2.5 - 3.4$ mm and $D = 3.6 - 4.5$ mm for H6, H1 and HF specimen respectively.

(2) By introducing a three dimensional defect size derived from two dimensional defect size, the effective prediction of the fatigue limit of the surface hardened specimen is possible. If large number of samples is considered for calculating the maximum defect size, the predicted maximum defect size is larger.

(3) Using the calculated maximum defect size, the lower fatigue limit can be predicted. In the case of the lower fatigue limit of HF specimen, the prediction is more conservative compared with H1 and H6 specimen. It is explained that high strength steel (HF specimen) can be failed at much longer lifetime compared with surface hardened specimen (H6 and H1 specimen).

References

1. N. E. FROST, K. J. MARSH and L. P. POOK, Metal Fatigue, (Oxford University Press, Oxford 1974).
2. H. KOBAYASHI and H. NISHIZAWA, *Trans. Jpn. Soc. Mech. Eng. A*, **36** (1969) 1856.
3. H. NORDBERG, in Proceeding Swedish Symposium on Non-Metallic Inclusions in Steel, (1981) 395.
4. M. H. EL HADDAD, K. N. SMITH and T. H. TOPPER, *Eng. Frac. Mech.* **11** (1979) 573.
5. J. E. SHIGLEY and C. R. MISCHKE, in "Mechanical Engineering Design", 5th Ed., (1989).
6. Y. MURAKAMI and M. ENDO, *Eng. Frac. Mech.* **17**(1) (1983) 1.
7. Y. MURAKAMI, S. KODAMA and S. KONUMA, *Int. J. Fatigue*, **11**(5) (1989) 291.
8. S. H. SONG and B. H. CHOI, *J. Mat. Sci.* **39**(1) (2004) 335.
9. Y. MURAKAMI and H. USUKI, *Int. J. Fatigue* **11**(5) (1989) 299.
10. *KS D0027*, Korean Standard (1999).
11. Y. KUROSHIMA, M. SHIMIZU and I. KAWASAKI, *Trans. JSME A*, **56** (**529**) (1999) 555.
12. T. TORIYAMA, Y. MURAKAMI and T. MAKINO, *J. Soc. Mater. Sci. Jpn.* **40** (1991) 1497.
13. H. USUKI and Y. MURAKAMI, *Trans. JSME A* **55**(510) (1989) 213.
14. T. SAKAI, *et al*, in Proc. of Int. Conf. 2001: fatigue in very high cycle region, (2001) 51.
15. T. MATSUMURA, Y. OCHI, S. YOSHIDA and K. MASAKI, in Proc. of ICF 10 (2001).

Received 6 November 2003
and accepted 25 March 2005